

Crater function moments: Role of implanted noble gas atomsGerhard Hobler,^{1,*} Dawid Maciążek,² and Zbigniew Postawa²¹*Institute of Solid-State Electronics, TU Wien, Floragasse 7, A-1040 Wien, Austria*²*Institute of Physics, Jagiellonian University, ul. Lojasiewicza 11, 30348 Kraków, Poland*

(Received 12 December 2017; revised manuscript received 5 April 2018; published 24 April 2018)

Spontaneous pattern formation by energetic ion beams is usually explained in terms of surface-curvature dependent sputtering and atom redistribution in the target. Recently, the effect of ion implantation on surface stability has been studied for nonvolatile ion species, but for the case of noble gas ion beams it has always been assumed that the implanted atoms can be neglected. In this work, we show by molecular dynamics (MD) and Monte Carlo (MC) simulations that this assumption is not valid in a wide range of implant conditions. Sequential-impact MD simulations are performed for 1-keV Ar, 2-keV Kr, and 2-keV Xe bombardments of Si, starting with a pure single-crystalline Si target and running impacts until sputtering equilibrium has been reached. The simulations demonstrate the importance of the implanted ions for crater-function estimates. The atomic volumes of Ar, Kr, and Xe in Si are found to be a factor of two larger than in the solid state. To extend the study to a wider range of energies, MC simulations are performed. We find that the role of the implanted ions increases with the ion energy although the increase is attenuated for the heavier ions. The analysis uses the crater function formalism specialized to the case of sputtering equilibrium.

DOI: [10.1103/PhysRevB.97.155307](https://doi.org/10.1103/PhysRevB.97.155307)**I. INTRODUCTION**

The crater function formalism [1–3] has recently established itself as an important technique in the theory of ion-beam induced spontaneous pattern formation. Earlier approaches used Sigmund’s theory of sputtering [4] together with a surface smoothing mechanism to derive equations of motion for the surface height function [5–8], some including simplified models of atom redistribution due to momentum transfer to target atoms [9–13]. Other work explains pattern formation in terms of mechanical stress [14–18]. In contrast, in the crater function formalism, the coefficients of the equation of motion are calculated in terms of the moments of the so-called crater function. The crater function is defined as the average response of the surface to a single ion impact [19] and may be obtained by molecular dynamics (MD) [19–22] or binary collision Monte Carlo (MC) simulations [23–26]. In this way, the crater function formalism allows to include the results of numerical simulations in the theory of spontaneous pattern formation.

In most previous work, using the crater function formalism, only sputtering and atom redistribution have been taken into account. The effect of the implanted ions on pattern formation has been investigated only recently [27,28]. It has been found that ion implantation has a destabilizing effect on the surface along the projected beam direction, if the incidence angle exceeds a critical value, while it always has a stabilizing effect in transverse direction. The impact of the implant contributions is expected to be particularly significant when erosion and redistribution are moderate such as for energetic light ions, and when the surface binding energy is high [28].

It is commonly assumed that the effect of the implanted ions on pattern formation is negligible, if the implanted atom species is a noble gas (NG). This is motivated by the fact that NG atoms have a tendency to leave the target [29], so the retained fluence is lower than for nonvolatile ions. Radiation induced transport of NG atoms towards the surface is well established experimentally [30] and has been named “rapid relocation” [31,32] in the absence of a clear understanding of the mechanism on an atomistic level. MC simulations cannot explain rapid relocation [33], thus it seems to be a nonballistic effect.

The rationale for neglecting implanted NG atoms in pattern formation, however, is flawed. First, the effect strongly depends on the system studied. For instance, while after 1-keV Ar bombardment of SiO₂ virtually no Ar is present in the oxide [32], for 5-keV Ne bombardment of ta-C [28] the experimentally found areal density of Ne agrees with that predicted by MC simulations. Second, the NG ions do not disappear instantaneously when they come to rest, but require additional ion bombardment to be transported (“rapidly relocated”) towards the surface. It will be shown that the separation of implantation and removal of the NG atoms leads to a contribution to the crater function.

The purpose of this work is to demonstrate that the implanted NG ions indeed have an important effect on the crater function moments. As a target we choose Si, which is a commonly studied material. Selected low-energy ion bombardments are investigated by MD simulations. MC simulations are used to study the effect in a wider range of impact energies. In the absence of a model for rapid relocation, MC simulations cannot predict the contribution of NG atom redistribution within the target. However, we will show that the net effect of the volumes added by the implanted ions and removed by their erosion is well predicted by MC simulations.

*gerhard.hobler@tuwien.ac.at

Our analysis will be based on the assumption of sputtering equilibrium. We therefore present the crater function formalism specialized to sputtering equilibrium in Sec. II. Details of the MD and MC methods employed are given in Sec. III. In Sec. IV, the MD and MC results are presented. Finally, in Sec. V we discuss the limitations of our approach and argue that they do not affect our qualitative conclusions.

II. CRATER FUNCTION FORMALISM

We start with a summary of the crater function formalism in order to define the nomenclature (Secs. IIA and IIB). Assumptions that are either normally made or are introduced by us, will be discussed in Sec. IIC. Their consequences for the calculation of the crater function moments will be presented in Secs. IID and IIE.

A. The crater function

In the crater function formalism, the equation of motion of the surface is written in terms of the moments of the crater function $F(x, y)$, where x is parallel to the projection of the beam direction to the originally flat surface, y is the surface coordinate perpendicular to x , and $x = y = 0$ corresponds to the impact point. The crater function is the average change in height due to the impact of a single ion. Different signs have been used for the crater function in previous work. When only erosion is considered, it is natural to define $F(x, y)$ as the negative change in surface height [2,28] so $F(x, y)$ is always positive. Here, we consider implantation and erosion on an equal footing. Therefore we prefer to adhere to the original convention introduced by Kalyanasundram *et al.* [19], which has also been used by Norris *et al.* [1,3], where erosion leads to negative and implantation to positive contributions to the crater function.

B. Crater function moments and surface stability

The i th moment with respect to x is defined by

$$M^{(i)} = \iint_{-\infty}^{\infty} x^i F(x, y) dx dy. \quad (1)$$

The crater function is composed of contributions from different atom species X and different mechanisms (erosion, redistribution, and implantation), so we can write

$$F(x, y) = \sum_X F_X(x, y) \quad (2)$$

with

$$F_X(x, y) = F_{X,\text{eros}}(x, y) + F_{X,\text{redist}}(x, y) + F_{X,\text{impl}}(x, y). \quad (3)$$

The same partitioning applies to the moments:

$$M^{(i)} = \sum_X M_X^{(i)} \quad (4)$$

with

$$M_X^{(i)} = M_{X,\text{eros}}^{(i)} + M_{X,\text{redist}}^{(i)} + M_{X,\text{impl}}^{(i)}. \quad (5)$$

Some of the contributions vanish by definition; for the zeroth moment, the contribution of atom redistribution is zero

if one assumes that the atomic volume does not change during relocation:

$$M_{X,\text{redist}}^{(0)} = 0. \quad (6)$$

Moreover, the target atom species $X \neq \text{NG}$, of course, have no implant contributions:

$$M_{X \neq \text{NG}, \text{impl}}^{(i)} = 0. \quad (7)$$

In the work, introducing the extended crater function formalism [2], the moments defined in Eq. (1) were written $M_x^{(i)}$ to distinguish them from moments with respect to y or curvature. However, in the final result, neither the moments with respect to y nor the moments with respect to curvature of order higher than zero appear. Zeroth-order moments are physically the same, independent of which quantity is considered variable. We have therefore dropped the index “ x ” in order to avoid confusion with X , which we use to denote atom species.

According to Harrison and Bradley, surface stability is determined by the curvature coefficients C_{11} and C_{22} given by [2]

$$C_{11} = \underbrace{\frac{\partial}{\partial \theta}(M^{(1)} \cos \theta)}_{S_{11}} + \underbrace{\frac{\partial}{\partial K_{11}}(M^{(0)} \cos \theta)}_{T_{11}} \quad (8)$$

and

$$C_{22} = \underbrace{\cot \theta (M^{(1)} \cos \theta)}_{S_{22}} + \underbrace{\frac{\partial}{\partial K_{22}}(M^{(0)} \cos \theta)}_{T_{22}}, \quad (9)$$

where θ denotes the incidence angle with respect to the surface normal and K_{11} , K_{22} the surface curvatures in x and y direction, respectively. The derivatives with respect to the curvatures are evaluated at zero curvature. Compared to Ref. [2], all terms appear with the opposite sign here due to the different sign conventions for the crater function. However, the meaning of C_{11} and C_{22} is the same as in Ref. [2]; instabilities occur when C_{11} and/or C_{22} is negative. Apart from the signs, the magnitudes of C_{11} and C_{22} are also of interest since the growth rate and velocity of the patterns in the linear regime depend on them [5]. As will be shown, $M^{(0)}$ is largely independent of the implanted ions in the cases studied, so the effect of the implanted ions on the stability of the surface is via S_{11} and S_{22} only [compare Eqs. (8) and (9)].

C. Assumptions

We will use the following assumptions as appropriate. (1) Each atom species X has a fixed atomic volume Ω_X that is known or can be determined and does not change during ion bombardment. (2) Sputtering equilibrium has been established, which means that the average rates of addition and removal of the ion species are equal. (3) The implanted ions do not affect the spatial characteristics of the collision cascades. (4) The spatial distribution of NG ejection with respect to the ion’s impact point is unaffected by rapid relocation.

Assumption 1 has first been made by Norris *et al.* [1] to arrive at a simplified algorithm for determining the moments from MD simulations (see Sec. IID). This algorithm is also the only known way to determine the moments from MC

simulations [23]. It is, however, not self-evident, in particular for NG atoms: when NG atoms are implanted, they are likely to initially end up in an interstitial position, while they usually form bubbles upon further bombardment [34]. The NG atoms do not necessarily have the same volume in these configurations, and the atomic volume is also not known *a priori*. Section IV B will address this in some detail.

Assumption 2 seems safe: sputtering equilibrium is reached for sputter depths on the order of the ions' projected range [35], while pattern formation usually requires higher fluences.

Assumption 3 can be valid only approximately: the different mass and volume of the implanted ions changes the stopping power of the target and therefore the spatial characteristics of the collision cascades. The effect is weaker the smaller the mass difference and the ion concentration. For the cases studied in this work (Ar, Kr, Xe in Si) we find from our MD simulations that assumption 3 is well fulfilled. Beyond these cases, we expect the effect of the implanted ions to increase with increasing implant energy, at lower implant angles, and when the rapid relocation effect is weaker, as all these conditions increase the implanted ion concentrations.

The rationale for assumption 4 is the following: the implanted NG atoms do not disappear immediately; otherwise, no NG concentration would be measured in the target. Instead, a thin near-surface region depleted from NG atoms is observed [31,32]. It is therefore reasonable to assume that the ejected NG atoms originate near this layer. Since the layer is thin, the properties of the collision cascade at these positions are similar as at the surface, and the spatial distribution of the ejected atoms is similar as in conventional sputtering.

D. Calculation and interpretation of the moments

With assumption 1, the crater functions may be approximated by sums of δ functions [1,3]

$$F(\mathbf{r}) = \sum_X \Omega_X \left\langle \sum_{i=1}^{n_X^F} \delta(\mathbf{r} - \mathbf{r}_{X_i}^F) - \sum_{i=1}^{n_X^I} \delta(\mathbf{r} - \mathbf{r}_{X_i}^I) \right\rangle, \quad (10)$$

where Ω_X is the atomic volume of atom species X (NG or Si, in our case), $\mathbf{r}_{X_i}^F = (x_{X_i}^F, y_{X_i}^F)$ denote the final positions of the n_X^F atoms of species X after the impact, $\mathbf{r}_{X_i}^I = (x_{X_i}^I, y_{X_i}^I)$ the initial positions of the n_X^I atoms of species X before the impact, and $\mathbf{r} = (x, y)$ the position where the crater function is evaluated. The atoms considered in Eq. (10) include only atoms in the target. This means, n_X^F includes the implanted ion if it ends up in the target, and the redistributed atoms. n_X^I includes the eroded and redistributed atoms. The angle brackets denote the average over a sufficient number of impacts.

Inserting Eq. (10) into Eq. (1), one obtains

$$M^{(0)} = \sum_X \Omega_X \langle n_X^F - n_X^I \rangle \quad (11)$$

$$M^{(1)} = \sum_X \Omega_X \left\langle \sum_{i=1}^{n_X^F} x_{X_i}^F - \sum_{i=1}^{n_X^I} x_{X_i}^I \right\rangle \quad (12)$$

The crater function as well as the moments may be decomposed into the contributions by the different atom species and physical mechanisms in an obvious way.

The contributions of implantation and erosion to the moments have simple physical meaning: $\langle n_{\text{NG}}^F \rangle_{\text{impl}}$ is one minus the reflection coefficient r_{NG} , thus

$$M_{\text{NG,impl}}^{(0)} = \Omega_{\text{NG}}(1 - r_{\text{NG}}), \quad (13)$$

while $M_{X \neq \text{NG,impl}}^{(0)} = 0$, see Eq. (7). $\langle n_X^I \rangle_{\text{eros}}$ is the partial sputtering yield Y_X , thus

$$M_{X,\text{eros}}^{(0)} = -\Omega_X Y_X. \quad (14)$$

Next, we observe that the contribution of ion implantation to the crater function is always positive, i.e., $F_{\text{NG,impl}}(x, y) \geq 0$ for all x and y . $F_{\text{NG,impl}}(x, y)/M_{\text{NG,impl}}^{(0)}$ may therefore be interpreted as the probability density that the end point of an ion trajectory has coordinates (x, y) . It follows that

$$\bar{x}_{\text{NG,impl}} = M_{\text{NG,impl}}^{(1)}/M_{\text{NG,impl}}^{(0)} \quad (15)$$

is the mean x coordinate of the ion trajectory end points. Similarly, $F_{X,\text{eros}}(x, y) \leq 0$ for all x and y , and $F_{X,\text{eros}}(x, y)/M_{X,\text{eros}}^{(0)}$, which is always positive, defines the probability density that the origin of a sputtered atom of type X has coordinates (x, y) . Therefore

$$\bar{x}_{X,\text{eros}} = M_{X,\text{eros}}^{(1)}/M_{X,\text{eros}}^{(0)} \quad (16)$$

is the mean x coordinate of the origins of sputtered X atoms. Henceforth, we will call $\bar{x}_{\text{NG,impl}}$ and $\bar{x}_{X,\text{eros}}$ the mean projected implant and erosion distance, respectively, where distance is meant to be defined with respect to the impact point. Note that $\bar{x}_{\text{NG,impl}}$ and $\bar{x}_{X,\text{eros}}$ are determined solely by the geometry of the collision cascades, while $M_{\text{NG,eros}}^{(0)}$ and $M_{\text{NG,eros}}^{(1)}$ are proportional to the near-surface concentrations of the NG atoms.

E. The moments in sputtering equilibrium

Assumption 2 means that the average number of implanted atoms per incident ion, which is one minus the reflection coefficient, equals the partial sputtering yield of the ion species:

$$1 - r_{\text{NG}} = Y_{\text{NG}}. \quad (17)$$

From Eqs. (13) and (14) follows

$$M_{\text{NG,eros}}^{(0)} = -M_{\text{NG,impl}}^{(0)}, \quad (18)$$

and because of Eqs. (5) and (6) the contribution of the implant species (NG) to the zeroth moment vanishes:

$$M_{\text{NG}}^{(0)} = 0. \quad (19)$$

The total zeroth moment is therefore given by

$$M^{(0)} = \sum_{X \neq \text{NG}} M_X^{(0)} = \sum_{X \neq \text{NG}} M_{X,\text{eros}}^{(0)}, \quad (20)$$

where in the last step Eqs. (6) and (7) have been used. Thus $M^{(0)}$ is simply minus the sum of the partial sputtering yields of the target atoms times the respective atomic volumes.

Introducing $M_{\text{NG,impl}}^{(1)}$ and $M_{\text{NG,eros}}^{(1)}$ from Eqs. (15) and (16), respectively, in Eq. (5) and using Eq. (18), the contribution of the implanted ions to the first moment can be written:

$$M_{\text{NG}}^{(1)} = (\bar{x}_{\text{NG,impl}} - \bar{x}_{\text{NG,eros}})M_{\text{NG,impl}}^{(0)} + M_{\text{NG,redist}}^{(1)}. \quad (21)$$

For the redistributed atoms, the number of initial and final positions within the target are equal ($n_{X,\text{redist}}$), and the contribution of redistribution of atom species X in Eq. (12) can be written:

$$M_{X,\text{redist}}^{(1)} = \Omega_X \left\langle \sum_{i=1}^{n_{X,\text{redist}}} (x_{Xi}^F - x_{Xi}^I) \right\rangle. \quad (22)$$

The sum is over all x components of the displacement vectors of the redistributed atoms. Because of momentum conservation, the average displacement must be in the direction of the incident ion. Therefore the sum is positive, and so is $M_{X,\text{redist}}^{(1)}$. Specializing to $X = \text{NG}$,

$$M_{\text{NG},\text{redist}}^{(1)} > 0 \quad (23)$$

follows, and from Eq. (21),

$$M_{\text{NG}}^{(1)} > (\bar{x}_{\text{NG,impl}} - \bar{x}_{\text{NG,eros}}) M_{\text{NG,impl}}^{(0)}. \quad (24)$$

Equation (24) specifies a lower limit to the contribution of the implanted NG atoms to the first moment. The importance of the assumption of sputtering equilibrium lies in the fact that all quantities on the right-hand side of Eq. (24) are independent of the implanted ion concentration, if this is the case for the geometry of the collision cascade (assumption 3) and the spatial distribution of NG ejection (assumption 4). This means that we now may use static MC simulations with a target containing a small constant concentration of NG atoms to determine at least a lower limit to the contribution of the implanted NG atoms to the first moment, even in the absence of a rapid relocation model. The only missing term in the NG contribution to the first moment, Eq. (21), then is $M_{\text{NG,redist}}^{(1)}$, which is proportional to the NG content. If, in addition, the contributions of the target atoms to the moments are independent of the NG content, then we may also estimate the other moment contributions using static MC simulations.

Note that an imbalance of the implant and erosion related contributions to the first moment, and thus a nonvanishing right-hand side of Eq. (24), implies that implantation and erosion are separate effects that have different spatial distributions. Our MD results presented in Sec. IV C validate this picture.

III. SIMULATION METHODS

A. Molecular dynamics simulations

MD simulations were carried out at Jagiellonian University using LAMMPS [36]. The simulation cell had a surface area of $28a \times 20a (\approx 152 \text{ \AA} \times 109 \text{ \AA})$, where $a = 5.431 \text{ \AA}$ is the lattice constant of Si, and the sample thickness was adjusted as to accommodate most of the collision cascades. The cell was initially filled with single-crystalline (100)-Si with a (2×1) reconstructed surface. Periodic boundary conditions were used in the lateral directions. Stochastic and rigid layers, 7 \AA and 3 \AA thick, respectively, were used at the bottom to simulate the thermal bath that kept the sample at the required temperature and to keep the shape of the sample. The simulations were run at 0 K temperature. The target was sequentially bombarded with 2-keV Kr ions at polar angles of 40° , 50° , 60° , 70° , 80° , and 85° and an azimuthal angle of 0° with respect to the cell edge, which is a [010] direction. In addition, one simulation was carried out each for 1-keV Ar and 2-keV Xe impacts

at an incidence angle of 60° . Each impact was simulated for 2 ps. The resulting structure was used as initial condition for the subsequent impact after removal of all sputtered atoms and any excess kinetic energy from the system. The latter was achieved by an energy quenching procedure that involved application of gentle viscotic forces to the entire sample for 5 ps. A Tersoff-3 potential [37] was used for Si-Si interactions, and the ZBL potential [38] for all other interactions (Kr-Kr, Ar-Ar, Xe-Xe, Kr-Si, Ar-Si, Xe-Si). Since the ZBL potential is known to overestimate the interaction at large interatomic separations, we also performed a simulation with the Süle potential for the Kr-Si and Kr-Kr interaction [39,40], which has been fitted to *ab initio* calculations. The Kr-Kr Süle potential is close to the well established HFD-B2 potential [41] in the eV energy range.

The sequential impact simulations take several weeks to run on a few dozens of CPUs for each incidence angle. It is quite obvious that such simulations currently cannot be performed for much higher impact energies, e.g., 200 keV, at reasonable expense. According to SRIM [42], the projected range R_p of Kr ions increases by a factor of 23 when going from 2 to 200 keV. To estimate the simulation time required for the MD simulation of a 200-keV Kr impact we assume that the cell size has to be scaled proportional to R_p in each dimension. This means that the number of atoms in the simulation and thus, roughly, the simulation time per impact increases as R_p^3 , i.e., by a factor of $23^3 \approx 1.2 \times 10^4$. In addition, the number of impacts required to reach sputtering equilibrium increases by about the same factor: to reach a certain fluence, the number of impacts scales with R_p^2 corresponding to the change in surface area. To reach sputtering equilibrium, a depth of $\sim R_p$ has to be sputtered [35]. Since the sputtering yield is only weakly dependent on the energy in the keV energy range [43], the fluence required to reach sputter equilibrium scales as R_p , and the number of impacts as R_p^3 . This motivates the use of MC simulations to investigate a wider range of impact energies.

B. Monte Carlo simulations

The sequential MD impact simulations correspond to a “dynamic mode” in MC parlance in that the changes to the target induced by one impact are taken into account in the next impact. Dynamic simulations are also performed with MC for the comparison of the retained fluence (Sec. IV A). For the MC simulations we use the IMSIL code [44,45]. The dynamic mode has been added to IMSIL some time ago based on the algorithm implemented in TRIDYN [46]. In this approach, the substrate is subdivided into slabs, whose thicknesses are adjusted periodically as to relax the atom densities to their equilibrium values. In our simulations, we used an initial slab thickness of 1 \AA and perform target relaxation after every 100 impacts, corresponding to a fluence increment of 10^{12} cm^{-2} . For reasons explained in Sec. III E, the MC simulations for the moments calculations are performed in static mode with a Si target containing a constant NG concentration of 2%.

In the MC simulations, atoms interacted via the Ziegler-Biersack-Littmark (ZBL) potential [38]. Electronic stopping was calculated using a mixed Lindhard/Oen-Robinson model [47,48] with Si parameters given in Ref. [49] and similar parameters for the NG. At low energies, electronic stopping plays only a minor role, since the Lindhard (nonlocal)

part is small at low energies [49], and the apsis of collision used in the Oen-Robinson model is always large. To obtain realistic sputtering yields, a planar potential barrier [50,51] corresponding to a surface binding energy of $E_s = 4.7$ eV is assumed for Si atoms and of $E_s = 0.25$ eV for the NG atoms. The former is chosen independent of the NG concentration contrary to the default model of IMSIL, as in reality we expect the near-surface region to deplete from the NG [32]. The surface binding energy for the NG atoms was chosen so that reduction towards smaller values did not change sputtering yields and $E_s \leq E_d$ (see below) was fulfilled. Unnecessarily low values of E_s should be avoided, since for the sake of a consistent model, trajectories are simulated down to a cutoff energy E_f equal to the minimum surface binding energy of all atoms, which leads to large simulation times if E_s is small. For the displacement energy E_d [38,52], a value of 0.25 eV was used in order to fit the first redistributive moments of MC to those of the MD simulations as much as possible without having to accept excessive simulation times. The use of a very low value of E_d is in line with earlier MC simulations within the crater function formalism [23].

C. Calculation of moments and derivatives

Since the crater functions are defined as the average response to a single ion, the moments have to be averaged over a number of impacts. In the MD simulations, we use 750 impacts for averaging, corresponding to a fluence increment of about 5×10^{14} cm $^{-2}$. The 750 impacts are either chosen after the first 375 impacts (“low fluence”) or as the last 750 impacts of a simulation (“steady state”). In the MC simulations, averaging is done over all impacts (usually 100 000) since there is no transient in the simulation.

As stated in Sec. II A, the origin of the coordinate system is defined by the impact point. Determination of the impact point in the MD simulations is complicated by the fact that surface roughness develops during bombardment (the typical RMS amplitude in our MD simulations is ~ 2 – 3 Å). In MD, we define the surface by moving a probe atom with radius 2.1 Å over the sample and taking the coordinates of the sample atom that is touched by the probe as the surface position. The impact point is taken as the intersection of the incoming ion direction with the average surface position. In the MC simulations, we define the surface position at the plane that divides the half spaces where target atoms are randomly generated or not.

We note that the definition of the impact point is relevant to the values of the first moment contributions by implantation and erosion ($M_{\text{NG,impl}}^{(1)}$ and $M_{\text{X,eros}}^{(1)}$, respectively), but it is irrelevant to the sum of the two NG contributions ($M_{\text{NG,impl}}^{(1)} + M_{\text{NG,eros}}^{(1)}$) in sputtering equilibrium, see Eq. (24). When comparing the individual contributions, however, e.g., between MD and MC, it is important to use consistent definitions.

The derivative with respect to the incidence angle θ occurring in the first term of Eq. (8) is calculated by fitting parabolas through three adjacent θ values, which is second-order accurate in $\Delta\theta$ [70]. Derivatives of the sputtering yield with respect to curvature are calculated by simulating sputtering from cylinders of radius $R = 5a$, where a is the mean depth of energy deposition at normal incidence, and taking the derivative equal

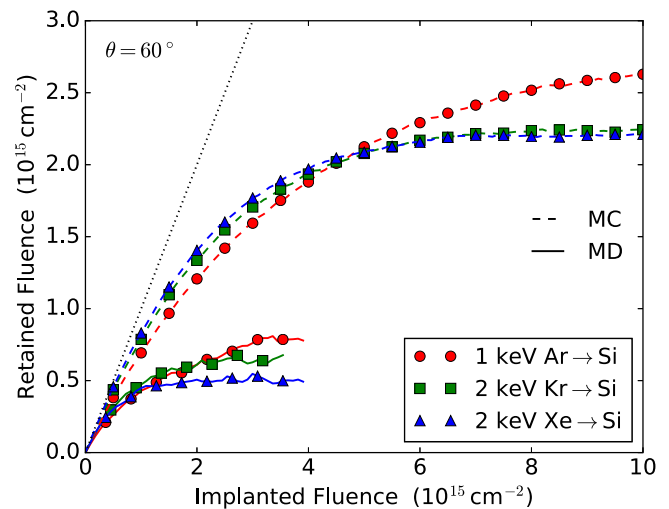


FIG. 1. Retained NG fluence as a function of implanted fluence for 1-keV Ar, 2-keV Kr, and 2-keV Xe bombardment of Si at an incidence angle of 60° as obtained with MD (solid lines) and MC simulations (dashed lines). Note the significantly higher steady-state retained fluence in the MC simulations than in MD.

to $-R$ times the difference in sputtering yield between cylinder and flat target [53].

It is difficult to do this with MD, since the dependence of the sputtering yield on the curvature becomes nonlinear for relatively little changes in the yield [71]. So, in order to approximate the derivative with respect to curvature by a difference quotient, small changes have to be evaluated, which require statistics that is expensive to obtain with MD. We will therefore use MC results for the terms T_{11} and T_{22} when reporting results for C_{11} and C_{22} .

IV. RESULTS

A. Retained fluence

Figure 1 shows the retained NG fluence as a function of implanted fluence for 1 keV Ar, 2 keV Kr, and 2 keV Xe bombardment of Si at an incidence angle of 60° . While all curves start at the origin with a slope close to unity (dotted line), indicating that little reflection occurs at this angle, they saturate at different levels: the MC steady-state values are more than a factor of three larger than the MD values. This can be assigned to the rapid relocation effect discussed in Ref. [31], which is not included in the MC simulations.

Figure 2 shows the Ar concentration depth profiles after 1 keV Ar bombardment of Si as predicted by MC and MD, compared to experimental data obtained by medium energy ion scattering (MEIS) [54]. Obviously, the MD simulations describe a large fraction of the rapid relocation effect. To check whether the remaining difference is due to insufficient simulation times, we annealed one sample at 600 K for 10 ns, and found a reduction in the retained NG fluence of only $\sim 10\%$ (this was done for 2-keV Kr at an incidence angle of 60°). This modification seems low enough to be neglected in our study. It also might be a real effect due to the elevated temperature.

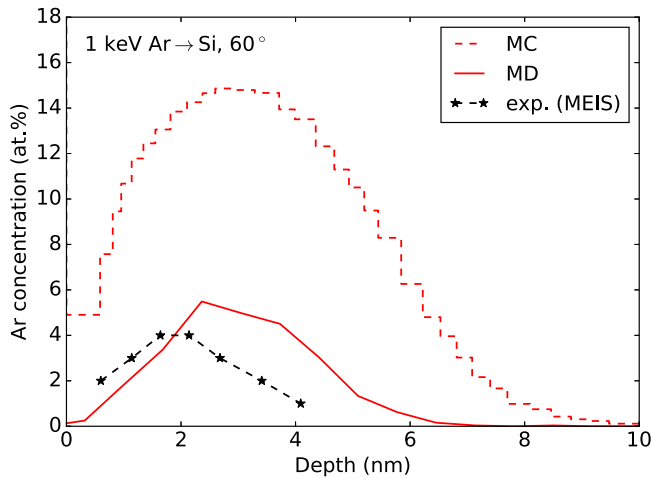


FIG. 2. Steady-state Ar concentration profiles after 1-keV Ar bombardment of Si as obtained with MD (solid line), MC (dashed line), and MEIS [54] (dashed line with symbols).

B. Atomic volume of the implanted species

According to Eqs. (10) to (12) the effect of the implanted ions on the crater function and its moments is proportional to their atomic volume. As a first guess, it might be plausible to use the densities in the liquid or solid phase [55]. However, bubbles are known to form during NG implantation, and the atomic density in the bubbles is uncertain. We have therefore determined the atomic density of the NG atoms by assuming a fixed value of $\Omega_{\text{Si}} = 20.4 \text{ \AA}^3$ for the atomic volume of amorphous Si [56] and fitting the NG atomic volume Ω_{NG} to the densities observed in the MD simulations. This is done by counting the NG and Si atoms (n_{NG} and n_{Si} , respectively) in a layer of thickness $4a \approx 21.7 \text{ \AA}$ at a depth of 1–4 nm below the surface. The known volume V of the slab must equal

$$V = n_{\text{NG}}\Omega_{\text{NG}} + n_{\text{Si}}\Omega_{\text{Si}}. \quad (25)$$

Plotting n_{Si} versus n_{NG} after each impact provides a point cloud to which Eq. (25) can be fitted by adjusting the only unknown Ω_{NG} . Since we are only interested in the steady state values, only the last 750 impacts are used for the fit.

In Fig. 3(a), the $n_{\text{Si}}(n_{\text{NG}})$ data are shown for 1-keV Ar, 2-keV Kr, and 2-keV Xe bombardment of Si at 60° . Each data set starts with $n_{\text{NG}} = 0$, $n_{\text{Si}} = 17920$, the situation before the first impact, and evolves towards the right. The first few impacts lead to a reduction in target density (strong decrease in n_{Si} with only moderate increase in n_{NG}), which is subsequently reversed. Closer inspection of the data shows that relaxation of the initial dilution occurs after 50–100 impacts (50 for Ar and 100 for Xe), corresponding to fluences around $5 \times 10^{13} \text{ cm}^{-2}$. This fluence is on the order of the amorphization threshold. The initial density reduction can be explained by the fact that target atoms are ejected from the near-surface region, where we measure the density, to either the vacuum or deeper parts of the target [57]. The subsequent increase of the target density is due to relaxation during amorphization. The last 750 data points in each set lead to the mean values and standard deviations of the atomic volumes given in the inset. The standard deviations might be slight underestimates caused by the limited impact

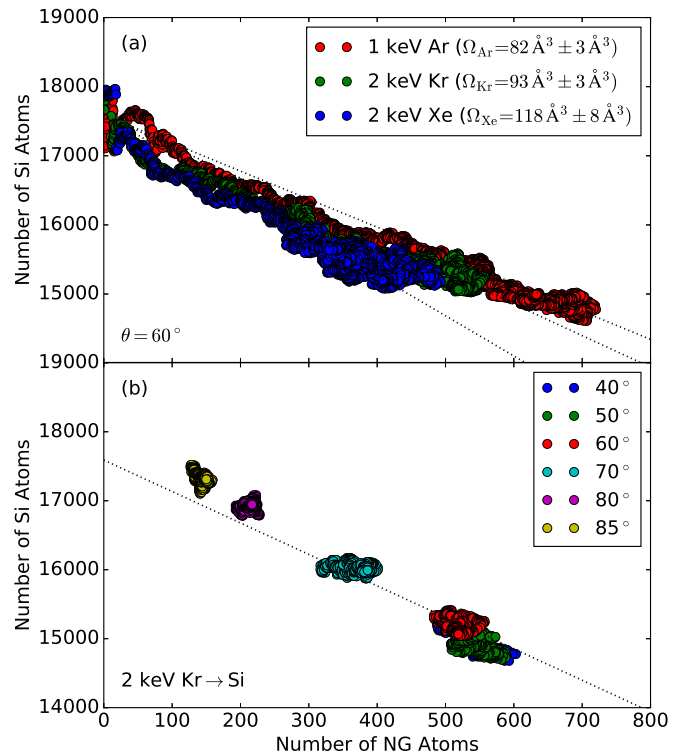


FIG. 3. Number of Si atoms vs number of NG atoms in a constant volume V (a) after each impact for 1-keV Ar, 2-keV Kr, and 2-keV Xe bombardment of Si at an incidence angle of 60° , and (b) after each of the last 750 impacts of 2-keV Kr at various incidence angles. The dotted lines are fits of the NG atomic volume to the last 750 impacts at 60° assuming the atomic volume of Si to equal the experimental value of $\Omega_{\text{Si}} = 20.4 \text{ \AA}^3$ [56].

intervals used for averaging. Choosing different 750-impact intervals after the first $\sim 5 \times 10^{14} \text{ cm}^{-2}$ (not shown), the atomic volumes are stable to within $\sim 10\%$.

Equation (25) with Ω_{Kr} fitted to the 60° data is shown in Fig. 3(b) together with the MD data for incidence angles between 40° and 85° (last 750 impacts). For incidence angles up to 70° the fit is excellent. For larger angles (80° and 85°), the MD data lie above the fit, which means that the material is denser than described by the fit. A possible explanation is that at the lower incidence angles bubbles form which have a somewhat lower density than small NG clusters and interstitial NG atoms. Bubbles are less likely to emerge at large incidence angles where the sputtering yield is high and the reflection coefficient is considerable.

The results for the atomic volumes Ω_{NG} are plotted in Fig. 4 together with published experimental data of solid state atomic volumes [55]. Our data exceed the solid state data by about a factor of two. To exclude an artifact of the ZBL interatomic potential, we have repeated the Kr simulation with the Sùle potentials. These potentials are weaker at large interatomic separations, so one would expect to obtain a smaller atomic volume. This is not the case within the statistical error, see the red symbol in Fig. 4. We conclude that the error introduced by the ZBL potential, if any, is quite moderate.

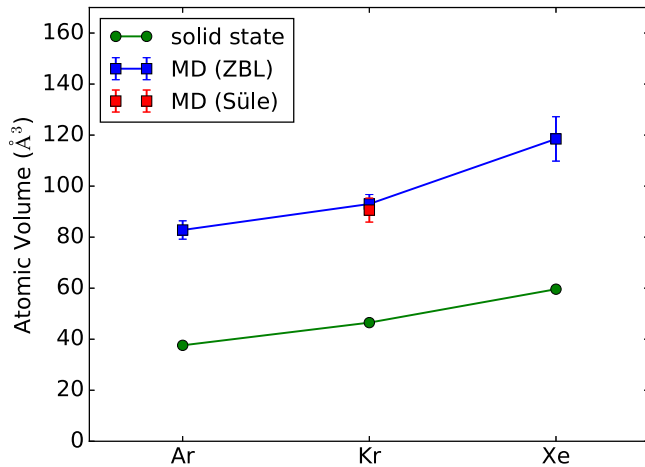


FIG. 4. Atomic volumes of Ar, Kr, and Xe as obtained by our MD simulations (squares with error bars) and experimental values in the solid state (green circles, [55]). In the MD simulations the NG-NG and NG-Si interatomic potentials have been chosen according to ZBL [38] (blue symbols and line) and Süle *et al.* [40] (red symbol). The lines are drawn to guide the eye.

The 600-K annealing described in Sec. IV A decreased the atomic volume by $\sim 10\%$ (not shown). We conclude that the atomic volumes are well determined in our MD simulations.

C. Effect of the implanted ions on the crater function moments: MD results

MD results for the contributions of implantation and erosion to the zeroth moment $M^{(0)}$ are shown in Fig. 5(a) as a function of incidence angle for 2-keV Kr bombardment of Si. As mentioned in Sec. II, atom redistribution does not contribute to the zeroth moment. Both “low-fluence” (dashed lines) and “steady-state” results (solid lines) as defined in Sec. III C are shown. Notably, the contributions of Si erosion and Kr implantation have hardly any fluence dependence, while the contribution of Kr erosion only gradually builds up as the Kr ions are implanted. In the high-fluence case, the erosive contribution of Kr is approximately the negative of its implant contribution, indicating that steady state has indeed been reached to a good degree.

Given these results, it is not surprising that the total zeroth moment in steady state [blue line labeled “total” in Fig. 5(b)] agrees well with the values of Si erosion alone (green curve labeled “Si only”). The remaining small difference is probably due to the fact that sputtering equilibrium has not completely been reached. The added Si and implant contribution (red curve labeled “Si + Kr implant”) is not a good approximation of the total zeroth moment in steady state.

As for the zeroth moment $M^{(0)}$, the contributions of Si erosion and Kr implantation to the first moment $M^{(1)}$ hardly depend on the fluence, see Fig. 6(a). The same holds true for the contribution by Si redistribution. Kr redistribution plays only a minor role, while the effect of Kr erosion on $M^{(1)}$ depends on fluence as expected: the influence of Kr erosion develops only gradually as Kr ions are implanted. However, in contrast to its contribution to $M^{(0)}$, the effect of Kr erosion is not completely compensated for in steady state by the effect of implantation.

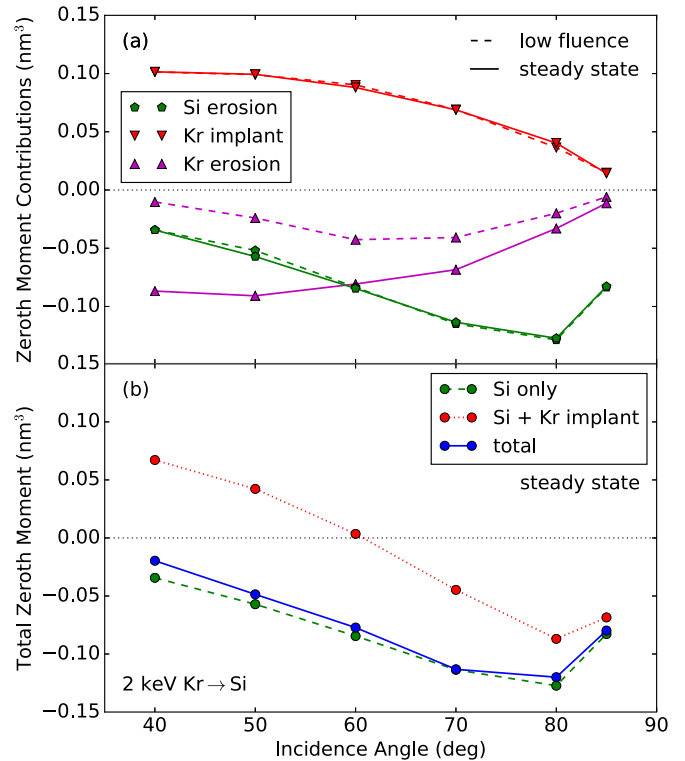


FIG. 5. MD results for the zeroth moment $M^{(0)}$ of the crater function of Si bombarded with 2 keV Kr vs incidence angle. (a) Contributions by implantation and erosion comparing low fluence and steady state; (b) sum of contributions in steady state. The difference between the blue solid line and the green dashed line in panel (b) should vanish in sputtering equilibrium.

According to Eq. (21), this would be the case if the mean projected implant distance $\bar{x}_{\text{Kr,impl}}$ equaled the mean projected erosion distance $\bar{x}_{\text{Kr,eros}}$. Rather, $M_{\text{Kr,impl}}^{(1)} > |M_{\text{Kr,eros}}^{(1)}|$ can be read from Fig. 6(a), and therefore $\bar{x}_{\text{Kr,impl}} > \bar{x}_{\text{Kr,eros}}$ validating, at least qualitatively, assumption 4.

As a consequence, the first moment in steady state does not agree well with the contributions of Si alone [solid blue and dashed green line, respectively, in Fig. 6(b)]. This is an important conclusion: the contribution of the implanted NG ions to the first moment is significant, on the order of 50% of the Si contribution in the present case.

Adding the Kr implant contribution to the Si contribution overestimates the total first moment $M^{(1)}$ [dotted red line in Fig. 6(b)]. Further adding the negative contribution of Kr erosion, thus neglecting only the redistributive contribution of the NG atoms, gives a lower limit to the total first moment $M^{(1)}$ (magenta line with triangles), see Eq. (24). For large angles it is a good approximation of $M^{(1)}$, while the deviation increases with decreasing incidence angle. In any case, it is a better approximation to $M^{(1)}$ than neglecting the Kr contributions altogether (dashed green line).

In Fig. 6(c), the curvature coefficient S_{11} is plotted as calculated from the data given in Fig. 6(b). As for $M^{(1)}$, the contribution of Kr to S_{11} is significant. Considering only the implant and erosive contributions (magenta line with triangles) is a reasonable approximation to the total values, although the deviation increases with decreasing incidence angle.

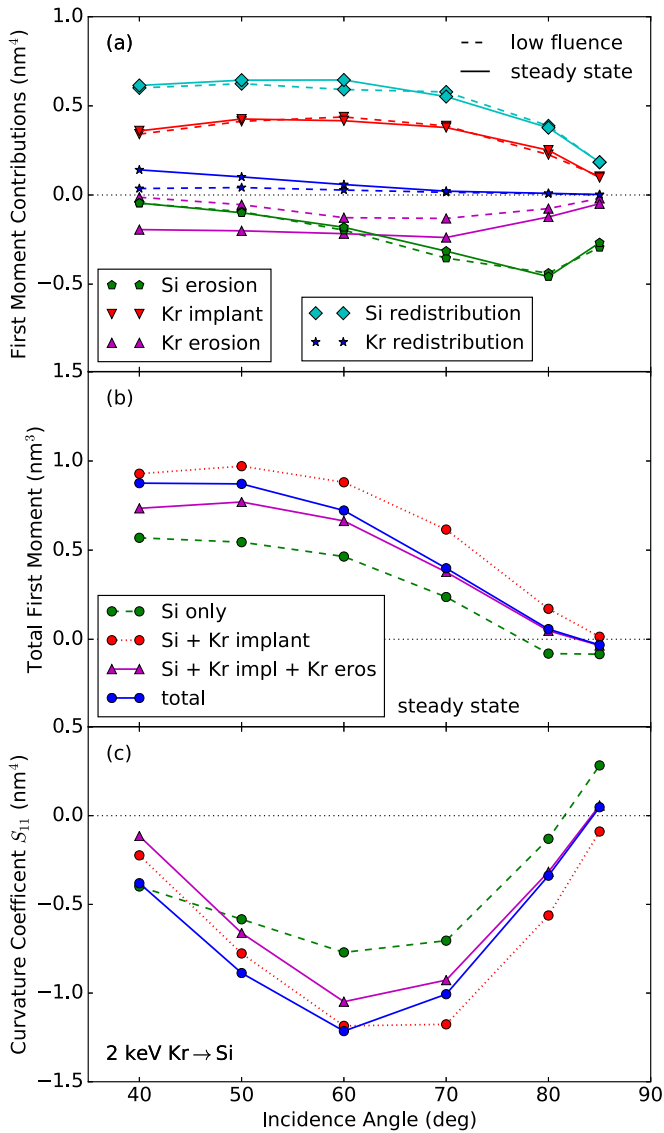


FIG. 6. MD results for the first moment $M^{(1)}$ of the crater function [(a) and (b)] and for the curvature coefficient S_{11} as defined in Sec. II (c) for Si bombarded with 2 keV Kr as a function of incidence angle. (a) Contributions by implantation, erosion, and redistribution; [(b) and (c)] sum of all contributions. For the meaning of the line styles see Fig. 5. In addition, results neglecting only the Kr erosive contribution [Eq. (24)] are shown by the magenta lines with triangles. The differences between the solid blue line and the dashed green line in (b) and (c) indicate the role of the implanted Kr ions.

Similar results for both the zeroth and first moment are also obtained for Ar and Xe ions, see Fig. 7. In all cases, the contribution of the implanted ions is significant, and the lower limit according to Eq. (24) is the best approximation to the full calculation.

Figure 8 shows three versions of the curvature coefficients C_{11} and C_{22} for the Kr case: according to the original crater function formalism considering only flat targets and Si atoms [1,21], according to the extended crater function formalism considering in addition the effect of surface curvature [2], and considering in addition the contributions of the Kr atoms as proposed in this work. As is obvious from

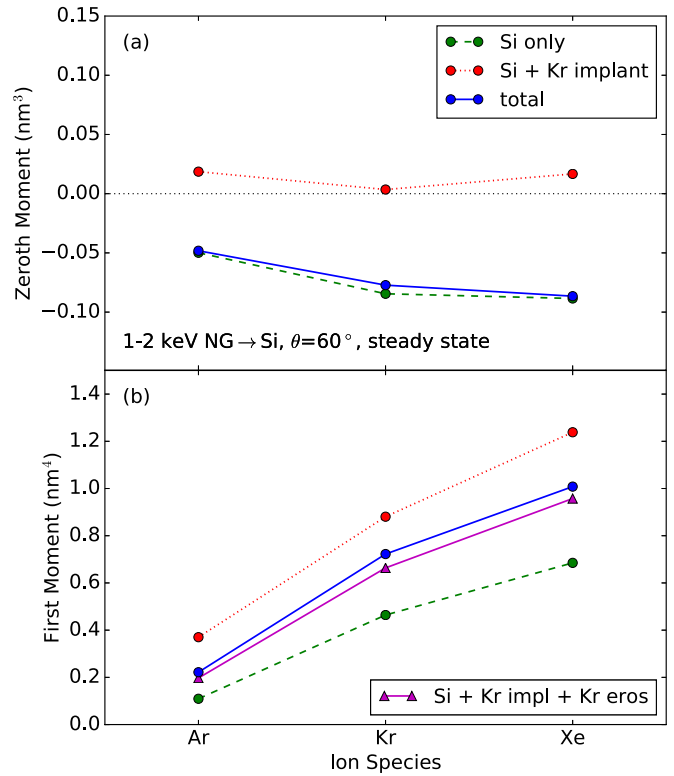


FIG. 7. Analogous to Figs. 5(b) and 6(b), but as a function of ion species for an incidence angle of 60° . For the meaning of the line styles see Fig. 6.

the plot, all contributions are significant. For C_{11} , the effect of surface curvature (the difference between the red dashed line and the green dotted line) partly compensates for the effect of the Kr atoms (difference between blue solid line and red dashed line), while for C_{22} both contributions work in the same direction.

D. MC versus MD results

As discussed in Sec. III A, the computational expense of MD simulations increases dramatically with increasing impact energy. To investigate the energy dependence of the role of the implanted ions, we have therefore performed MC simulations as described in Sec. III B. We recall that it is not possible to reliably predict the NG concentration in the target using MC simulations. As a consequence, there is uncertainty for the redistributive and erosive NG contributions to the first moment. The redistributive contribution has turned out to be small in the cases studied [Figs. 6(a) and 7(b)] and will therefore be neglected. The erosive contribution can be approximated assuming sputtering equilibrium and that the mean erosion distance does not depend on the details of the NG profile in the target. We use a Si target with a constant Kr concentration of 2% for our calculations.

In Fig. 9, MD and MC results of the contributions to the first moment according to Eq. (24) are compared (magenta triangles connected by solid and dashed lines, respectively), showing good agreement. Towards lower incidence angles this approximation increasingly underestimates the total Kr contribution [blue circles, Fig. 9(a)] as the Kr redistributive contribution

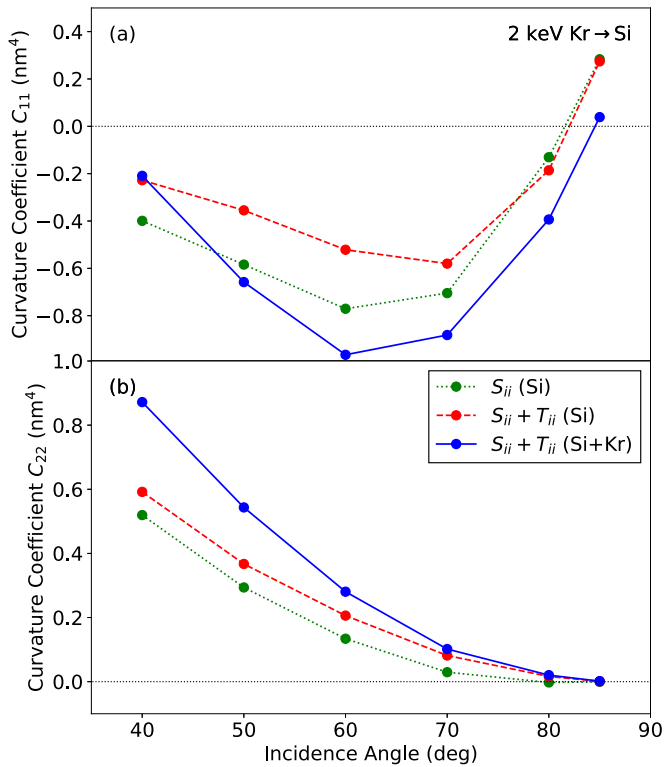


FIG. 8. MD results for the curvature coefficients (a) C_{11} and (b) C_{22} for 2-keV Kr bombardment of Si considering only flat targets and Si atoms [S_{ii} (Si), green dotted lines], considering in addition the effect of surface curvature [$S_{ii} + T_{ii}$ (Si), red dashed lines], and considering all contributions including those of the NG atoms as proposed in this work [$S_{ii} + T_{ii}$ (Si+Kr), blue solid lines]. Note that the first zero of C_{11} would occur at $\theta < 40^\circ$ if data points at smaller incidence angles were added.

increases [compare also Fig. 6(b)]. For comparison, the Si redistributive contributions are also shown. The MD and MC results are similar, but again somewhat diverge towards smaller incidence angles. Figure 9(b) shows similar agreement for the lighter Ar and the heavier Xe ions. The ion mass dependence of the Si redistributive contribution is somewhat underestimated by MC, which may be explained by a spike effect [58] not included in the MC simulations.

The two critical quantities in Eq. (24) are the mean projected distances of the implant positions $\bar{x}_{\text{NG,impl}}$ and the erosion points $\bar{x}_{\text{NG,eros}}$ from the impact point. The distributions of these distances for 60° Kr impacts at 2 keV are plotted in Fig. 10(a). Good agreement between the MD and MC results is observed. Very clearly, the average implant distance is larger than the average erosion distance, i.e., implantation takes place considerably further away from the impact point than sputtering. This is plausible as nuclear energy is preferably deposited in a narrow region close to the impact point (see Fig. 15 of Ref. [59]). According to Eq. (21), $\bar{x}_{\text{NG,impl}} > \bar{x}_{\text{NG,eros}} > 0$ means that the added contributions of NG erosion and implantation are positive but smaller than the contribution by implantation alone.

The agreement between the MD results, which include the rapid relocation effect, and the MC results, which do not, is remarkable also because it confirms the picture proposed in as-

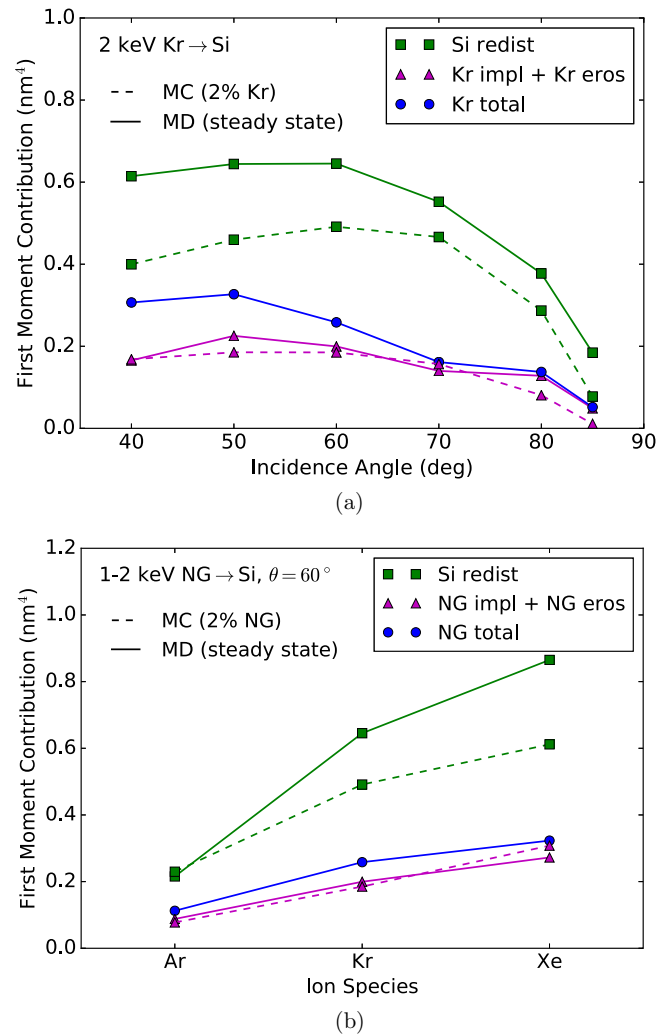
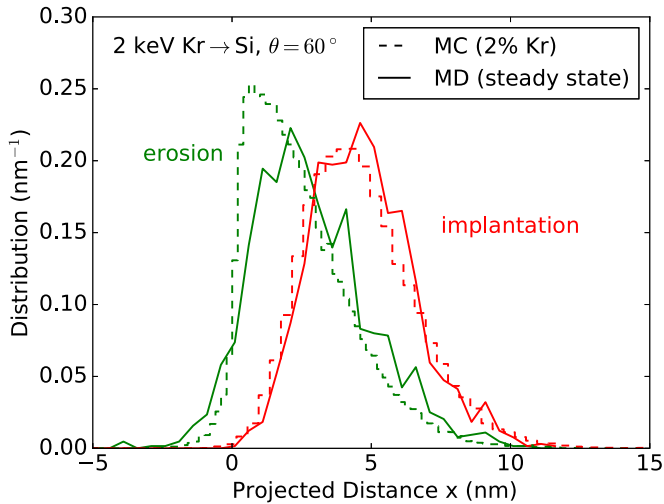


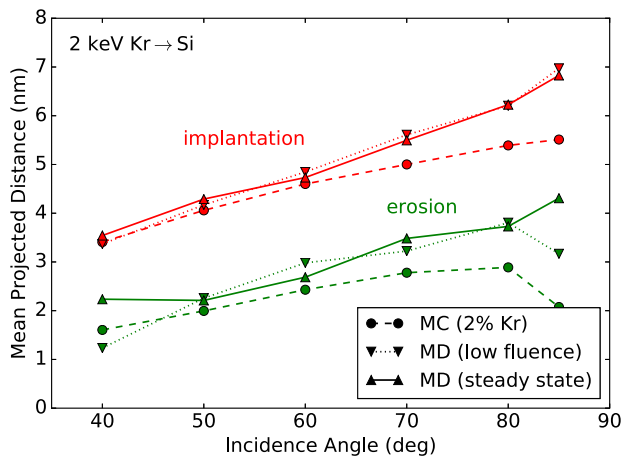
FIG. 9. Contributions of the NG (blue circles) and Si (green squares) to the first moment $M^{(1)}$ as obtained by MD (solid lines) and MC simulations (dashed lines). In addition, the implant plus erosive contributions of Kr are shown by the magenta triangles. (a) 2-keV Kr as a function of incidence angle; (b) for an incidence angle of 60° as a function of ion species (1-keV Ar, 2-keV Kr, and 2-keV Xe).

sumption 4 of Sec. II C: while the NG atoms are driven towards the surface by rapid relocation, their eventual sputtering has similar spatial properties as in the absence of rapid relocation.

In Fig. 10(b), these quantities are compared as a function of incidence angle. Excellent agreement is found for angles up to 60°, while MC and MD results moderately diverge at larger angles. However, all that matters to the added effect of implantation and erosion is the difference between $\bar{x}_{\text{NG,impl}}$ and $\bar{x}_{\text{NG,eros}}$, which agrees well between MC and MD also for the larger angles. This also explains why the added contributions of Kr implantation and Kr erosion to the first moment (magenta lines in Fig. 9) agree well between MD and MC. The MD results in Fig. 10(b) also show that the mean projected implant and erosion distances hardly depend on the fluence, compare the solid and dotted lines. This confirms that $\bar{x}_{\text{NG,impl}}$ and $\bar{x}_{\text{NG,eros}}$ are robust quantities that may be calculated without exact knowledge of the NG concentration in the target.



(a)



(b)

FIG. 10. (a) Distribution of the projected distance from the impact point ($=x$ coordinate) for 2-keV Kr bombardment of Si at an incidence angle of 60° ; (b) mean projected distance from the impact point as a function of incidence angle for 2 keV Kr bombardment of Si. Red lines: implanted ions; green lines: sputtered Kr atoms. Solid lines: MD in steady state; dashed lines: MC; dotted lines: MD at low fluence. In (a), the MD results have been averaged over the last 1500 ion impacts.

E. MC results for a wider range of impact conditions

The ion species and energy dependence of $\bar{x}_{\text{NG,impl}}$ and $\bar{x}_{\text{NG,eros}}$ as calculated by our MC simulations for an incidence angle of 60° is shown in Fig. 11. Note that always $\bar{x}_{\text{NG,impl}} > \bar{x}_{\text{NG,eros}}$. According to Eq. (24) this means that the added contributions of NG implantation and erosion on the first moment are always positive. Both quantities increase with energy, and this is also true of their ratio $\bar{x}_{\text{NG,impl}}/\bar{x}_{\text{NG,eros}}$. While $\bar{x}_{\text{NG,impl}}/\bar{x}_{\text{NG,eros}}$ is only 1.33, 1.57, and 1.88 at 200 eV for Ar, Kr, and Xe ions, respectively, it exceeds a factor of three at 200 keV.

The importance of the implanted ions to the crater function must of course be related to the contributions of the target atoms. In Fig. 12, we therefore compare the curvature coefficients C_{11} and C_{22} with and without consideration of

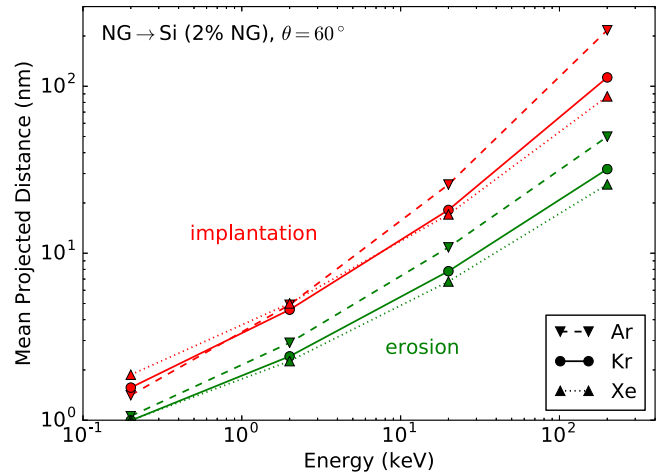


FIG. 11. MC results for the mean projected distances from the impact point for the implanted ions ($\bar{x}_{\text{NG,impl}}$, red lines and symbols) and for the sputtered atoms ($\bar{x}_{\text{NG,eros}}$, green lines and symbols) as a function of impact energy. Data for the three ion species Ar, Kr, and Xe at an incidence angle of 60° are shown.

the NG atoms (solid and dashed lines, respectively), where the contribution of the NG atoms has been estimated using Eq. (24). Data are given as a function of incidence angle for three ion species (Ar, Kr, and Xe) and four energies (0.2, 2, 20, and 200 keV). The effect of the implanted NG ions is significant in all cases, increases with impact energy although the increase is attenuated for the heavier ions. In all cases the ions have a destabilizing effect on the surface with respect to parallel mode ripples (contribution to $C_{11} < 0$) for incidence angles larger than 40° – 50° up to at least 85° . They do not change the lower critical angle for parallel mode ripple formation [zero of $C_{11}(\theta)$] significantly, but move the upper critical angle to higher values. On the other hand, the ions always have a stabilizing effect on the surface with respect to perpendicular mode ripples (contribution to $C_{22} > 0$). These results are qualitatively the same as for self-implantation [27,28].

V. DISCUSSION AND CONCLUSION

From the results presented in the previous section, we conclude that the implanted NG ions in general play an important role in determining crater function moments. The rationale may be summarized as follows: (i) the average projected distance of the implanted ions from the impact point, measured along the surface, is larger than the corresponding average distance of the sputtered atoms. This leads to incomplete compensation of the effects of ion implantation and erosion on the first moment. (ii) Redistribution of the implanted ions due to subsequent impacts is always away from the impact point and therefore can only add to (rather than compensate for) the effect of ion implantation. (iii) The average atomic volumes of the NG atoms have been found in our MD simulations to be approximately twice those of the NG atoms in the solid state. This means that their effect on the crater function moments is twice that one would obtain with the solid state volumes.

There are some uncertainties in the simulations; however, they do not compromise our conclusion. First, MD may only

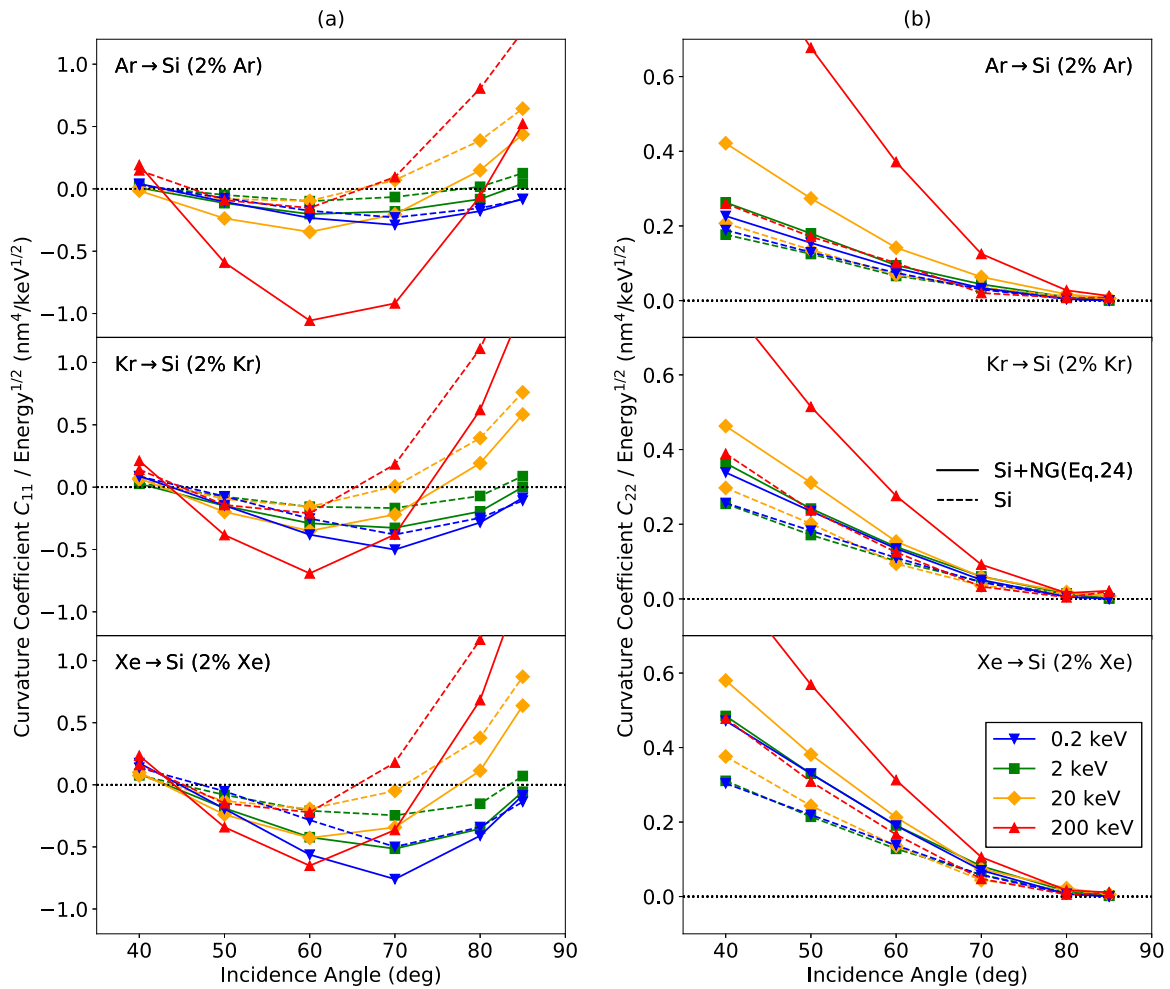


FIG. 12. MC results for the curvature coefficients (a) C_{11} and (b) C_{22} , comparing simulations with and without consideration of the effect of the implanted NG ions (solid and dashed lines, respectively). Data are shown for Si bombarded with Ar, Kr, and Xe at energies of 0.2, 2, 20, and 200 keV as a function of incidence angle. The results have been scaled with the square root of the impact energy to better represent them in the plots.

describe effects that occur on the timescale of the collision cascades. Thermally activated processes that mainly operate between the collision cascades are not included. While a systematic understanding of the effect of temperature on pattern formation is still lacking [60], there are indications that temperature does have an effect, even not too far from room temperature [61–65]. Also, thermally activated NG diffusion could explain the differences between the Ar concentration profiles obtained by MD and experimentally, see Fig. 2, although our annealing simulation did not provide enough evidence for a thermal effect. Anyway, thermal effects do not influence the range of the implanted ions and thus the implant contribution to the first crater function moment. Moreover, NG redistribution would be reduced, if the NG concentrations in the target were decreased by thermal diffusion, but our argument is not based on the redistributive NG contribution, which is small in our MD simulations and has been neglected in the MC simulations.

Second, MC simulations have their inaccuracies due to the binary collision approximation. As a result, the ion mass dependence of redistribution is underestimated by MC, see the Si redistribution results in Fig. 9(b). This is reminiscent of the ion mass dependence of damage formation in crystalline

Si, which is explained by the increasing relevance of thermal spikes with increasing ion mass [58]. However, the effect is moderate and is not expected to increase with ion energy: higher impact energies add high-energy portions to the ion trajectories, which are well described in the binary collision approximation.

Another consequence of the binary collision approximation is its failure to describe the rapid relocation effect that leads to an overestimation of the retained NG fluence, see Fig. 2. The retained fluence is expected to increase with ion energy [31]. Therefore one may expect an increasing contribution of NG redistribution to the first crater function moment with increasing energy. This would further enhance the importance of the implanted NG atoms beyond the analysis given in Sec. IV E. The argument is not so straightforward, however, since the other contributions to the first moment also increase with energy. The issue could be clarified by using a rapid relocation model [33] in the MC simulations that is fitted to experimental data on the retained fluence where such data is available. Again, NG redistribution would only add to the effects of implantation and erosion, so it would only increase the importance of the implanted ions.

As mentioned in Sec. IIC, our MC simulations are based on the assumption that it is not necessary to know the exact concentration of the implanted NG atom (or that the actual concentration is close to the assumed one). This assumption is not perfectly valid. For instance, the sputtering yield increases by 25% from a pure Si target to steady state for 140-keV or 270-keV Xe bombardments [66]. This is explained by a reduction in ion and recoil range by the implanted heavy Xe atoms. This also means that the mean projected implant and erosion distances ($\bar{x}_{\text{NG,impl}}$ and $\bar{x}_{\text{NG,eros}}$) both shrink, which would not invalidate our analysis. It should also be taken into account that the ion species and energy in this study [66] represent extreme cases in view of the present study, and that this experiment was done at normal incidence, while we are more interested in oblique incidence where NG gas retention is reduced.

Before finishing, a few words on how our calculated curvature coefficients compare to experiments seem appropriate. From a qualitative point of view, all levels of sophistication of the crater function formalism [considering planar surfaces only [1], including the effect of curvature [2], and including the effect of the implanted NG atoms (this work)] agree with experiments performed under impurity-free conditions [60], in that they predict parallel mode ripple formation ($C_{11} < 0$) for incidence angles above a critical angle around 45° up to another critical angle at grazing incidence. On closer examination, several discrepancies manifest themselves. For instance, the very careful experiments on 2-keV Kr bombardment of Si by Engler *et al.* [67] yielded a lower critical angle of 58° , significantly larger than 45° . For Ar ions, it has been found that no ripples occur for ion energies of 3 to 10 keV [26] in contrast to the predictions of the crater function formalisms. Finally, perpendicular mode ripples have been measured for 10-keV Xe bombardment at an incidence angle of 80° [68], while our MC results do not predict perpendicular mode ripple formation ($C_{22} < 0$) at any of the investigated conditions. Unfortunately, we cannot report resolution of these discrepancies due to consideration of the effect of the implanted ions. On the other hand, the crater function formalism is intuitive, and MD and MC simulations are well-established techniques. We therefore believe that the cause of the discrepancy lies outside the crater function formalism, possibly in

stress effects operating in the amorphous layer on a scale not covered by MD simulations [15–18].

Finally, we wish to comment on a recent study of pattern formation by 1-MeV Au in Ti and its alloy TiAlV [69]. Applying our MC analysis to these conditions, we arrive at exactly the same conclusions as the authors of Ref. [69]. The relative importance of the implanted ions is close to negligible (results not shown). Au is about 50% heavier than Xe, which might be the cause why the implanted ions can be neglected in spite of the high impact energy. This also indicates that our conclusion about the importance of the implanted NG ions might not apply to Rn, the only NG heavier than Xe, which is even heavier than Au.

Au, of course, is not a NG, and Au implanted at this high energy is substantially incorporated in the target as demonstrated in Ref. [69] by RBS measurements. Such conditions should be analyzed by dynamic MC simulations, which would predict the implanted ion depth profile. In these simulations the redistributive contribution of the implanted ions to the first moment would be significant. This contribution could be determined with confidence, since depth profiles of nonvolatile ions are well predicted by MC simulations; the “rapid relocation” effect is a phenomenon associated with NG atoms only.

Our main finding in this work is that due to the difference between the mean projected implant and erosion distances ($\bar{x}_{\text{NG,impl}} - \bar{x}_{\text{NG,eros}}$) the implanted NG ions usually play a role comparable to those of sputtering and atom redistribution as evaluated by crater functions. This is the case even though NG atoms are rapidly removed from the target so that their concentration is low at any time. While there are still open questions in the modeling of ion-target interaction that must be solved to make quantitative predictions, the fact that $\bar{x}_{\text{NG,impl}} - \bar{x}_{\text{NG,eros}}$ agrees well between MD and MC simulations (Fig. 10) is strong support for this conclusion to be true not only at the conditions investigated by MD but also at higher energies.

ACKNOWLEDGMENTS

We gratefully acknowledge R. M. Bradley for helpful discussions. D.M. and Z.P. would like to gratefully acknowledge the financial support from the Polish National Science Center, Program 2015/19/B/ST4/01892.

-
- [1] S. A. Norris, M. P. Brenner, and M. J. Aziz, *J. Phys.: Condens. Matter* **21**, 224017 (2009).
 - [2] M. P. Harrison and R. M. Bradley, *Phys. Rev. B* **89**, 245401 (2014).
 - [3] S. A. Norris, J. Samela, M. Vestberg, K. Nordlund, and M. J. Aziz, *Nucl. Instrum. Methods B* **318**, 245 (2014).
 - [4] P. Sigmund, *J. Mater. Sci.* **8**, 1545 (1973).
 - [5] R. M. Bradley and J. M. E. Harper, *J. Vac. Sci. Technol. A* **6**, 2390 (1988).
 - [6] R. Cuerno and A.-L. Barabási, *Phys. Rev. Lett.* **74**, 4746 (1995).
 - [7] M. A. Makeev, R. Cuerno, and A.-L. Barabasi, *Nucl. Instrum. Methods Phys. Res. B* **197**, 185 (2002).
 - [8] J. Muñoz-García, R. Cuerno, and M. Castro, *Phys. Rev. B* **78**, 205408 (2008).
 - [9] G. Carter and V. Vishnyakov, *Phys. Rev. B* **54**, 17647 (1996).
 - [10] T. Aste and U. Valbusa, *New J. Phys.* **7**, 122 (2005).
 - [11] B. Davidovitch, M. J. Aziz, and M. P. Brenner, *Phys. Rev. B* **76**, 205420 (2007).
 - [12] O. Bobes, K. Zhang, and H. Hofsäss, *Phys. Rev. B* **86**, 235414 (2012).
 - [13] S. Numazawa and R. Smith, *J. Phys.: Condens. Matter* **25**, 095003 (2013).
 - [14] N. V. Medhekar, W. L. Chan, V. B. Shenoy, and E. Chason, *J. Phys.: Condens. Matter* **21**, 224021 (2009).
 - [15] M. Castro, R. Gago, L. Vázquez, J. Muñoz-García, and R. Cuerno, *Phys. Rev. B* **86**, 214107 (2012).
 - [16] M. Castro and R. Cuerno, *Appl. Surf. Sci.* **258**, 4171 (2012).
 - [17] S. A. Norris, *Phys. Rev. B* **86**, 235405 (2012).

- [18] S. A. Norris, J. C. Perkinson, M. Mokhtarzadeh, E. Anzenberg, M. J. Aziz, and K. F. Ludwig, *Sci. Rep.* **7**, 2016 (2017).
- [19] N. Kalyanasundaram, M. Ghazisaeidi, J. B. Freund, and H. T. Johnson, *Appl. Phys. Lett.* **92**, 131909 (2008).
- [20] N. Kalyanasundaram, J. B. Freund, and H. T. Johnson, *J. Phys.: Condens. Matter* **21**, 224018 (2009).
- [21] S. A. Norris, J. Samela, L. Bukonte, M. Backman, F. Djurabekova, K. Nordlund, C. S. Madi, M. P. Brenner, and M. J. Aziz, *Nat. Commun.* **2**, 276 (2011).
- [22] M. Z. Hossain, K. Das, J. B. Freund, and H. T. Johnson, *Appl. Phys. Lett.* **99**, 151913 (2011).
- [23] H. Hofsäss, *Appl. Phys. A* **114**, 401 (2014).
- [24] H. Hofsäss, *Appl. Phys. A* **119**, 687 (2015).
- [25] O. El-Atwani, S. A. Norris, K. Ludwig, S. Gonderman, and J. P. Allain, *Sci. Rep.* **5**, 18207 (2015).
- [26] H. Hofsäss, O. Bobes, and K. Zhang, *J. Appl. Phys.* **119**, 035302 (2016).
- [27] R. M. Bradley and H. Hofsäss, *J. Appl. Phys.* **120**, 074302 (2016).
- [28] H. Hofsäss, K. Zhang, and O. Bobes, *J. Appl. Phys.* **120**, 135308 (2016).
- [29] P. Blank, K. Wittmaack, and F. Schulz, *Nucl. Instrum. Methods* **132**, 387 (1976).
- [30] N. Menzel and K. Wittmaack, *Nucl. Instrum. Methods B* **7**, 366 (1985).
- [31] K. Wittmaack, *Nucl. Instrum. Methods B* **267**, 2846 (2009).
- [32] K. Wittmaack, A. Giordani, R. Umbel, and J. L. Hunter, Jr., *J. Vac. Sci. Technol. A* **34**, 051404 (2016).
- [33] A. Mutzke and W. Eckstein, *Nucl. Instrum. Methods B* **266**, 872 (2008).
- [34] K. Wittmaack and H. Oppolzer, *Nucl. Instrum. Methods B* **269**, 380 (2011).
- [35] M. Nastasi and J. W. Mayer, *Ion Implantation and Synthesis of Materials* (Springer, Berlin, Heidelberg, 2006).
- [36] S. Plimpton, *J. Comput. Phys.* **117**, 1 (1995).
- [37] J. Tersoff, *Phys. Rev. B* **39**, 5566 (1989).
- [38] J. F. Ziegler, J. P. Biersack, and U. Littmark, *The Stopping and Range of Ions in Solids* (Pergamon Press, New York, 1985).
- [39] P. Süle and K.-H. Heinig, *J. Chem. Phys.* **131**, 204704 (2009).
- [40] P. Süle, [arXiv:1401.1612](https://arxiv.org/abs/1401.1612) [cond-mat.mtrl-sci].
- [41] A. K. Dham, W. J. Meath, A. R. Allnatt, R. A. Aziz, and M. J. Slaman, *Chem. Phys.* **142**, 173 (1990).
- [42] J. F. Ziegler, SRIM-2013 software package, available online at <http://www.srim.org>.
- [43] W. Eckstein, in *Sputtering by Particle Bombardment*, edited by R. Behrisch and W. Eckstein, Topics in Applied Physics, Vol. 110 (Springer, Berlin, Heidelberg, 2007), pp. 33–189.
- [44] G. Hobler, *Nucl. Instrum. Methods B* **96**, 155 (1995).
- [45] C. Ebm and G. Hobler, *Nucl. Instrum. Methods B* **267**, 2987 (2009).
- [46] W. Möller, W. Eckstein, and J. Biersack, *Comput. Phys. Commun.* **51**, 355 (1988).
- [47] J. Lindhard and M. Scharff, *Phys. Rev.* **124**, 128 (1961).
- [48] O. S. Oen and M. T. Robinson, *Nucl. Instrum. Methods* **132**, 647 (1976).
- [49] G. Hobler and C. Murthy, in *2000 International Conference on Ion Implantation Technology Proceedings* (IEEE, Piscataway, 2000), pp. 209–212.
- [50] P. Sigmund, *Phys. Rev.* **184**, 383 (1969).
- [51] W. Eckstein, *Computer Simulation of Ion-Solid Interactions* (Springer, Berlin, 1991).
- [52] G. H. Kinchin and R. S. Pease, *Rep. Prog. Phys.* **18**, 1 (1955).
- [53] H. M. Urbassek, R. M. Bradley, M. L. Niemiadi, and W. Möller, *Phys. Rev. B* **91**, 165418 (2015).
- [54] D. W. Oh, S. K. Oh, H. J. Kang, H. I. Lee, and D. W. Moon, *Nucl. Instrum. Methods B* **190**, 598 (2002).
- [55] WebElements, <http://www.webelements.com>, accessed 20 June, 2017.
- [56] J. S. Custer, M. O. Thompson, D. C. Jacobson, J. M. Poate, S. Roorda, W. C. Sinke, and F. Spaepen, *Appl. Phys. Lett.* **64**, 437 (1994).
- [57] G. Hobler, in *Process Physics and Modeling in Semiconductor Technology*, edited by G. R. Srinivasan, C. S. Murthy, and S. T. Dunham (The Electrochem. Soc., Pennington, 1996), pp. 509–521.
- [58] M.-J. Caturla, T. Díaz de la Rubia, L. A. Marqués, and G. H. Gilmer, *Phys. Rev. B* **54**, 16683 (1996).
- [59] G. Hobler, R. M. Bradley, and H. M. Urbassek, *Phys. Rev. B* **93**, 205443 (2016).
- [60] J. Muñoz García, L. Vázquez, M. Castro, R. Gago, A. Redondo-Cubero, A. Moreno-Barrado, and R. Cuerno, *Mater. Sci. Eng. R* **86**, 1 (2014).
- [61] G. Carter, V. Vishnyakov, Y. V. Martynenko, and M. J. Nobes, *J. Appl. Phys.* **78**, 3559 (1995).
- [62] G. Carter, V. Vishnyakov, and M. J. Nobes, *Nucl. Instrum. Methods B* **115**, 440 (1996).
- [63] C. C. Umbach, R. L. Headrick, and K.-C. Chang, *Phys. Rev. Lett.* **87**, 246104 (2001).
- [64] R. Banerjee, S. Hazra, and M. K. Sanyal, *J. Phys. D: Appl. Phys.* **41**, 055306 (2008).
- [65] D. Chowdhury, B. Satpati, and D. Ghose, *Mater. Res. Express* **3**, 125003 (2016).
- [66] P. Blank and K. Wittmaack, *J. Appl. Phys.* **50**, 1519 (1979).
- [67] M. Engler, S. Macko, F. Frost, and T. Michely, *Phys. Rev. B* **89**, 245412 (2014).
- [68] K. Zhang, F. Rotter, M. Uhrmacher, C. Ronning, H. Hofsäss, and J. Krauser, *Surf. Coat. Technol.* **201**, 8299 (2007).
- [69] M. A. Garcia, J. Rickards, R. Cuerno, R. Trejo-Luna, J. Cañetas-Ortega, L. R. de la Vega, and L. Rodríguez-Fernández, *Phys. Rev. Appl.* **8**, 064027 (2017).
- [70] This algorithm is also used in the gradient function of NUMPY, see <http://www.numpy.org>.
- [71] For example, for 20-keV Ar in Si, nonlinearity with respect to curvature becomes significant when the sputtering yield has changed by $\sim 10\%$, see Fig. 4(a) of Ref. [53].